Acta Crystallographica Section D
Biological Crystallography
ISSN 0907-4449

The crystal structures of native and (*S*)-lysine-bound dihydrodipicolinate synthase from *Escherichia coli* with improved resolution show new features of biological significance

Renwick C. J. Dobson,[a]‡ Michael D. W. Griffin,[a]‡ Geoffrey B. Jameson[b] and Juliet A. Gerrard[a]*

[a]School of Biological Sciences, University of Canterbury, Christchurch, New Zealand, and [b]Centre for Structural Biology, Institute of Fundamental Sciences, Massey University, Palmerston North, New Zealand

‡ These authors contributed equally to this work.

Correspondence e-mail: juliet.gerrard@canterbury.ac.nz

Received 6 March 2005
Accepted 20 May 2005

PDB References: dihydrodipicolinate synthase, native, 1yxc, r1yxcsf; dihydrodipicolinate synthase, (*S*)-lysine bound, 1yxd, r1yxdsf.

Dihydrodipicolinate synthase (DHDPS) mediates the key first reaction common to the biosynthesis of (*S*)-lysine and *meso*-diaminopimelate. The activity of DHDPS is allosterically regulated by the feedback inhibitor (*S*)-lysine. The crystal structure of DHDPS from *Escherichia coli* has previously been published, but to only a resolution of 2.5 Å, and the structure of the lysine-bound adduct was known to only 2.94 Å resolution. Here, the crystal structures of native and (*S*)-lysine-bound dihydrodipicolinate synthase from *E. coli* are presented to 1.9 and 2.0 Å, respectively, resolutions that allow, in particular, more accurate definition of the protein structure. The general architecture of the active site is found to be consistent with previously determined structures, but with some important differences. Arg138, which is situated at the entrance of the active site and is thought to be involved in substrate binding, has an altered conformation and is connected *via* a water molecule to Tyr133 of the active-site catalytic triad. This suggests a hitherto unknown function for Arg138 in the DHDPS mechanism. Additionally, a re-evaluation of the dimer–dimer interface reveals a more extensive network of interactions than first thought. Of particular interest is the higher resolution structure of DHDPS with (*S*)-lysine bound at the allosteric site, which is remote to the active site, although connected to it by a chain of conserved water molecules. (*S*)-Lysine has a slightly altered conformation from that originally determined and does not appear to alter the DHDPS structure as others have reported.

1. Introduction

Dihydrodipicolinate synthase (DHDPS; EC 4.2.1.52) mediates the key first step common to the biosynthesis of (*S*)-lysine and *meso*-diaminopimelate: the condensation of (*S*)-aspartate-β-semialdehyde [(*S*)-ASA] and pyruvate to form (4*S*)-4-hydroxy-2,3,4,5-tetrahydro-(2*S*)-dipicolinic acid (HTPA) (Fig. 1). This reaction is under allosteric control by the feedback inhibitor (*S*)-lysine. As DHDPS is expressed in plants and microorganisms, but not in animals, it attracts continued attention as a target for antibiotics and herbicides (Coulter *et al.*, 1999; Cox *et al.*, 2000; Hutton *et al.*, 2003), but no potent inhibitor has yet been found. As the purported rate-deter-

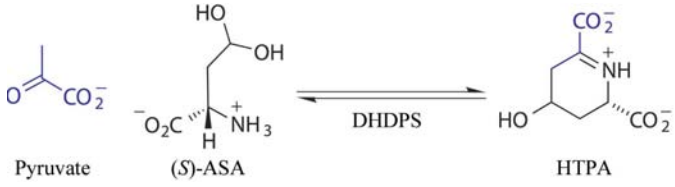

Figure 1
Reaction catalysed by dihydrodipicolinate synthase (DHDPS).

mining step in (*S*)-lysine biosynthesis, DHDPS also attracts the attention of biotechnologists aiming to engineer crops rich in (*S*)-lysine, often the limiting nutrient in staple crops (Miflin *et al.*, 1999). For these reasons, DHDPS has attracted sustained interest in the literature since its first characterization (Yugari & Gilvarg, 1965). However, success in these fields has been limited, at least in part owing to the poor knowledge of the complexities in the mechanism and regulation of DHDPS activity.

The product of the condensation of (*S*)-ASA and pyruvate is currently thought to be the unstable heterocycle (4*S*)-4-hydroxy-2,3,4,5-tetrahydro-(2*S*)-dipicolinic acid (HTPA), although this is still uncertain. Fig. 2 outlines the currently accepted mechanism of DHDPS (Blickling *et al.*, 1997; Hutton *et al.*, 2003). In the first step, the active-site lysine (Lys161 in *Escherichia coli* DHDPS) forms a Schiff base with pyruvate, as has been unequivocally demonstrated in several studies (Borthwick *et al.*, 1995; Laber *et al.*, 1992; Shedlarski & Gilvarg, 1970). Subsequent binding of the second substrate, presumed to be the hydrated form of (*S*)-ASA (Coulter *et al.*, 1996; Tudor *et al.*, 1993), is followed by dehydration and cyclization to form the product. Although in aqueous solution (*S*)-ASA is known to exist predominantly in the hydrated form rather than the aldehyde (Coulter *et al.*, 1996; Tudor *et al.*, 1993), the biologically relevant form of the substrate remains to be determined. Based on the X-ray crystal structure of the *E. coli* enzyme (Blickling *et al.*, 1997; Mirwaldt *et al.*, 1995), sequence homologies with DHDPS from other sources (Lawrence *et al.*, 1997) and site-directed mutagenesis studies (Dobson, Valegård *et al.*, 2004), it is proposed that a catalytic triad of three residues, Tyr133, Thr44 and Tyr107 (*E. coli* numbering), acts as a proton relay to transfer protons to (and from) the active site *via* a water-filled channel leading to the (*S*)-lysine-binding site and to the bulk solvent. The recently deposited although unpublished structure of DHDPS from *Thermotoga maritima* (PDB code 1o5k) reinforces these conclusions.

Importantly for the regulated biosynthesis of *meso*-diaminopimelate and (*S*)-lysine, the DHDPS reaction has been shown to be feedback regulated by (*S*)-lysine (Dobson, Gerrard *et al.*, 2004; Yugari & Gilvarg, 1965). In the aspartate family of amino acids, (*S*)-lysine biosynthesis appears to be controlled at two points. The first is the feedback inhibition of one isozyme of aspartate kinase (AK) by lysine. The second

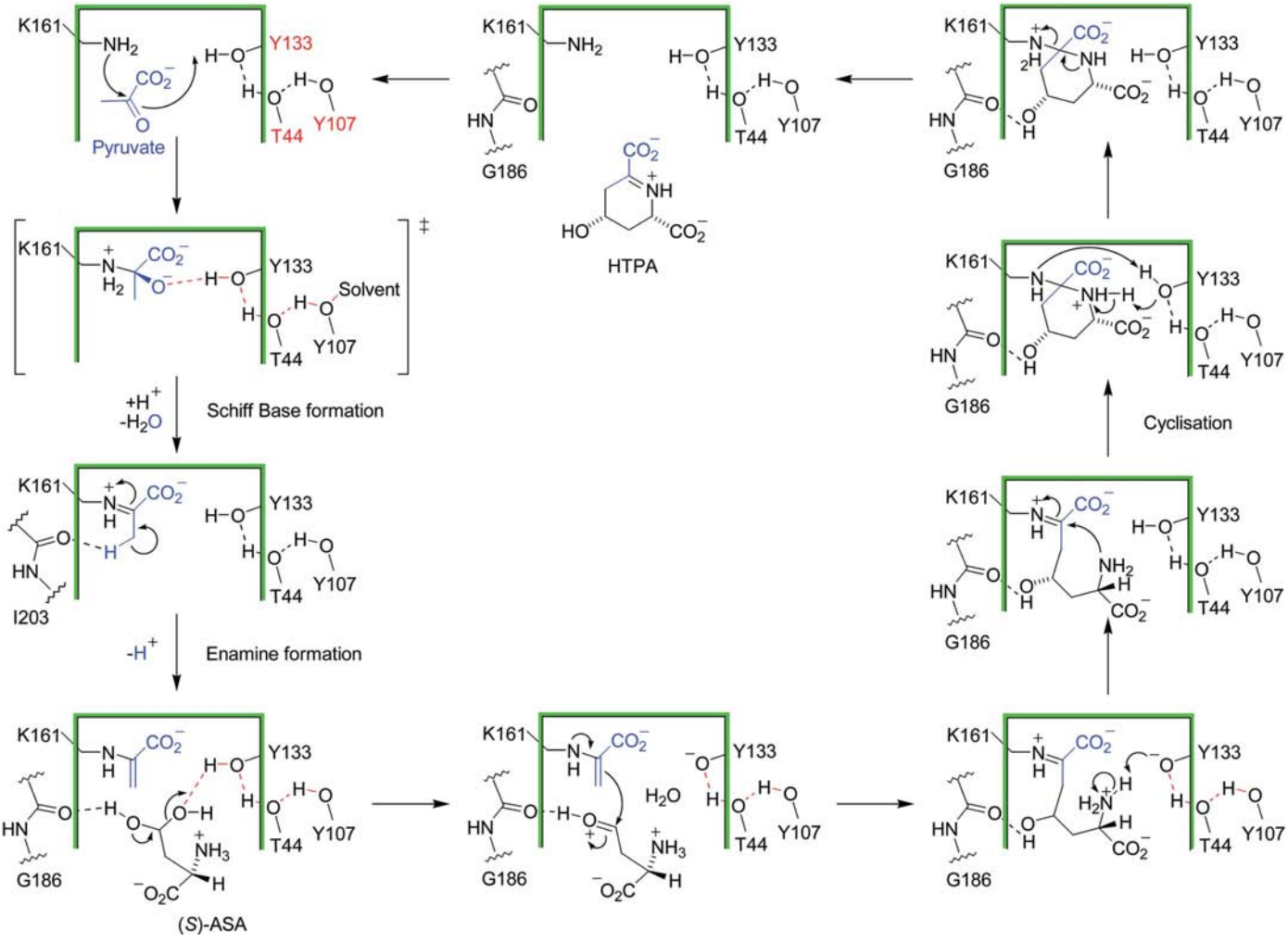

Figure 2
Currently accepted mechanism of DHDPS.

Table 1
Data set and refinement statistics.

Values in parentheses are for the highest resolution shell.

	Native DHDPS	DHDPS + (*S*)-lysine
Resolution (data processing) (Å)	1.90 (1.97–1.90)	2.00 (2.07–2.00)
No. of images	240	360
Oscillation range (°)	0.3	0.5
Space group	$P3_121$	$P3_121$
Unit-cell parameters (Å)	a = 121.87, b = 121.87, c = 110.19	a = 121.15, b = 121.15, c = 110.08
No. of reflections/unique reflections	314877/73225	688649/63306
Completeness (%)	99.7 (99.9)	100.0 (100.0)
$R_{\rm merge}$†	0.089 (0.358)	0.088 (0.356)
$I/\sigma(I)$	9.7 (3.5)	14.9 (6.1)
Resolution (refinement) (Å)	1.90 (1.949–1.900)	2.00 (2.052–2.000)
$R_{\rm free}$‡	0.211 (0.348)	0.186 (0.241)
$R_{\rm cryst}$§	0.172 (0.266)	0.159 (0.205)
Mean B value (Å^2)	19.9	19.9
Estimated coordinate error¶	0.079	0.073
Residues/solvent molecules	584/616	584/557
R.m.s.d. from ideal geometry		
Bond lengths (Å)	0.015	0.014
Bond angles (°)	1.6	1.5

† $R_{\rm merge} = \sum|I - \langle I\rangle|/\sum\langle I\rangle$. ‡ $R_{\rm free}$ is based on 5.1% of the total reflections excluded from refinement. § $R_{\rm cryst} = \sum||F_{\rm obs}| - |F_{\rm calc}||/\sum|F_{\rm obs}|$. ¶ Based on maximum-likelihood calculations.

control point is DHDPS, the first reaction unique to lysine biosynthesis. In plants, two lines of evidence suggest that DHDPS is the rate-limiting step. Firstly, DHDPS has greater sensitivity to lysine ($K_{\rm i}$ = 5–50 µ*M*) in comparison to AK ($K_{\rm i}$ = 200–600 µ*M*) (Galili, 1995; Karchi *et al.*, 1995) and secondly expression of lysine-insensitive AK in plants results in the accumulation of threonine, not lysine, whereas expression of lysine-insensitive DHDPS results in the accumulation of (*S*)-lysine (Galili, 1995, 2002).

Depending on their regulatory properties with respect to (*S*)-lysine, isozymes of DHDPS can be grouped into three classes (Blickling *et al.*, 1997). Plant enzymes are strongly inhibited by (*S*)-lysine (IC_{50} = 0.01–0.05 m*M*), such as the DHDPS from *Triticum aestivium* (Kumpaisal *et al.*, 1989), *Daucus carota sativa* (Mathews & Widholm, 1978), *Spinacia oleracea* (Wallsgrove & Mazelis, 1981), *Nicotiana sylvestris* (Ghislain *et al.*, 1990), *Zea mays* (Frisch *et al.*, 1991) and *Pisum sativum* (Dereppe *et al.*, 1992). Enzymes from Gram-negative bacteria such as *E. coli* (Yugari & Gilvarg, 1965), *Bacillus sphaericus* (Bartlett & White, 1986) and *Methanobacterium thermoautotrophicum* (Bakhiet *et al.*, 1984) are only weakly inhibited, with an IC_{50} between 0.25 and 1.0 m*M*. DHDPS from Gram-positive bacteria appear not to be inhibited by (*S*)-lysine at all (IC_{50} = 10 m*M*). For example, little or no feedback inhibition by (*S*)-lysine was observed for DHDPS from bacteria such as *B. licheniformis* (Stahly, 1969), *B. megaterium* (Webster & Lechowich, 1970), *B. subtilis* (Yamakura *et al.*, 1974), *Corynebacterium glutamicum* (Cremer *et al.*, 1990), *B. cereus* (Hoganson & Stahly, 1975) and *B. lactofermentum* (Tosaka & Takinami, 1978).

The mechanism by which (*S*)-lysine exerts regulatory control over DHDPS from *E. coli* is not well understood, although kinetic and structural studies support the proposal that (*S*)-lysine is an allosteric inhibitor (Blickling *et al.*, 1997, 1998; Kumpaisal *et al.*, 1989; Laber *et al.*, 1992; Stahly, 1969; Yugari & Gilvarg, 1965). A structural study of the plant DHDPS from *N. sylvestris* suggests that the mechanism of inhibition involves an altered quaternary structure upon (*S*)-lysine binding (Blickling *et al.*, 1998). This is not thought to be the case in the *E. coli* enzyme, which has a different quaternary architecture to the *N. sylvestris* enzyme (Blickling *et al.*, 1998).

The native enzyme has been solved previously by X-ray diffraction methods to moderate resolution (2.5 Å), whereas that of the (*S*)-lysine-bound structure has only been solved to a resolution of 2.94 Å. Critical in any study of enzyme mechanism is the availability of high-resolution structures, especially with bound ligands. In this study, we present the structures of *E. coli* DHDPS with and without bound (*S*)-lysine to resolutions of at least 2.0 Å.

2. Methods and materials

2.1. Expression and purification of DHDPS

DHDPS was expressed from an *E. coli* XL-1 Blue cell line harbouring the plasmid pJG001, as previously described (Dobson, Gerrard *et al.*, 2004; Dobson, Griffin *et al.*, 2004). The purification methods were modified to incorporate aspects from Mirwaldt *et al.* (1995) with the following modifications: pyruvate was not added to the crude extract prior to sonication, the heat-shock step was performed in 1.5 ml Eppendorf tubes with 1 ml aliquots and the FPLC step was omitted, since the purified DHDPS afforded crystals without this step.

The native enzyme was purified 5.7-fold to a specific activity of 1.8 µ$M_{\rm NADPH}$ s^{-1} mg^{-1} and was homogeneous as judged by SDS–PAGE with Coomassie Blue staining (Dobson, Griffin *et al.*, 2004). Kinetic characterization of wild-type DHDPS yielded kinetic parameters consistent with previous literature reports (Coulter *et al.*, 1999; Karsten, 1997; Yugari & Gilvarg, 1965): the data fitted the ping-pong kinetic mechanism and yielded a $k_{\rm cat}$ equal to 124 ± 6.8 s^{-1} (at 303 K) and Michaelis–Menten constants for pyruvate and (*S*)-ASA of 0.26 ± 0.03 m*M* and 0.11 ± 0.01 m*M*, respectively (Dobson, Griffin *et al.*, 2004).

2.2. Crystallization and ligand soaking

The crystallization experiments were undertaken as described by Mirwaldt *et al.* (1995) using the hanging-drop vapour-diffusion method at 277 K. Each drop contained 3 µl protein solution (~8 mg ml^{-1} in 20 m*M* Tris–HCl pH 8), 1.2 µl precipitant (1.8 *M* K_2HPO_4 pH 10) and 0.6 µl *N*-octyl-β-*R*-glucopyranoside [6%(*w*/*v*)]. Crystals appeared after 3–4 d and grew to dimensions of up to 0.3 mm. For the (*S*)-lysine-bound structure, crystals were soaked in mother liquor with 100 m*M* (*S*)-lysine for 3–4 d. Prior to X-ray data collection, the crystals were soaked in cryoprotectant solution [1.8 *M* K_2HPO_4 pH 10,

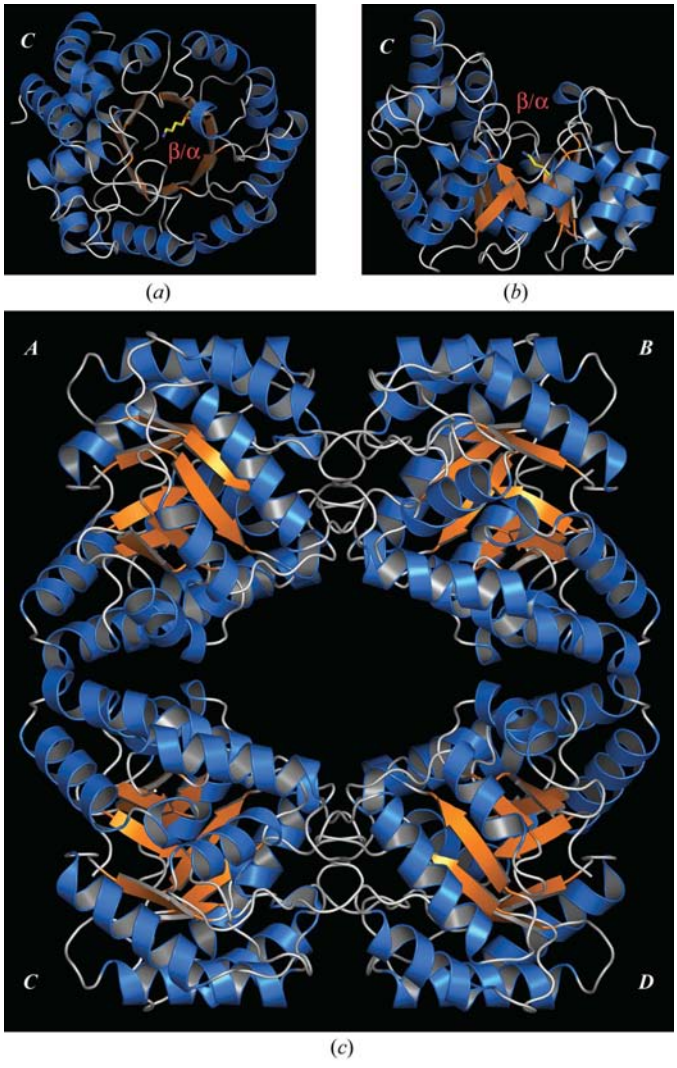

Figure 3
Tertiary and quaternary structure of DHDPS. (*a*) View looking down the $(\beta/\alpha)_8$-barrel and C-terminal domain. The active site is defined by the position of Lys161 (stick view). (*b*) Side view of the $(\beta/\alpha)_8$-barrel and C-terminal domain. (*c*) The quaternary structure. Monomers *A* and *B* make up the asymmetric unit. This and subsequent figures were produced using *PyMOL* (DeLano, 2002) unless stated otherwise.

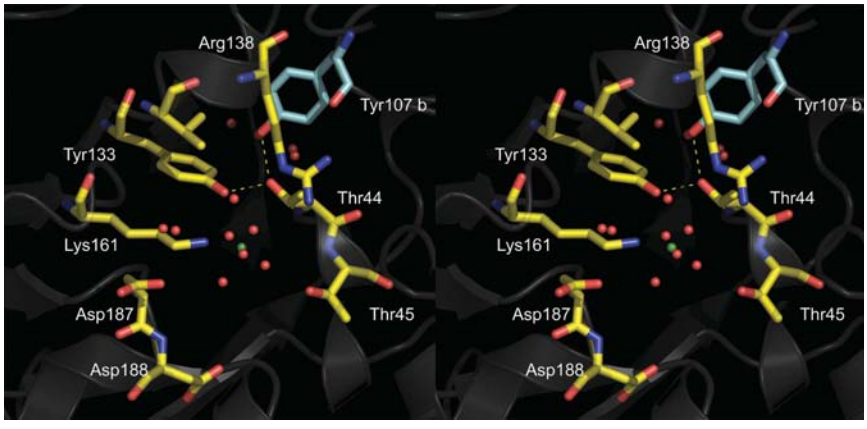

Figure 4
Stereo plot of the active site of DHDPS.

20%(*v*/*v*) glycerol including 100 m*M* (*S*)-lysine where appropriate] and directly flash-frozen in liquid nitrogen.

2.3. Data collection and processing

Intensity data were collected at 110 K using an R-AXIS IV^{++} image-plate detector coupled to a Rigaku Micromax 007 X-ray generator operating at 40 kV and 20 mA. The crystals belong to space group $P3_121$ and diffract to beyond 1.8 and 2.0 Å resolution for the native and (*S*)-lysine-bound DHDPS crystals, respectively. Diffraction data sets were processed and scaled using the program *CrystalClear* (Pflugrath, 1999). The merging *R* values were 0.088 and 0.089 for the native and (*S*)-lysine-bound data sets, respectively (Table 1). The unit-cell parameters were consistent with those published previously (Blickling *et al.*, 1997; Dobson, Valegård *et al.*, 2004; Mirwaldt *et al.*, 1995).

2.4. Structure determination and refinement

The location and orientation of the native DHDPS structure was confirmed within the unit cell using *AMoRe* (Navaza & Saludjian, 1997), where the search model was the *E. coli* DHDPS monomer (PDB code 1dhp). The (*S*)-lysine-bound structure was solved, again with *AMoRe*, using our refined native structure. Refinement was achieved using *REFMAC*5 (Collaborative Computational Project, Number 4, 1994) with manual model corrections using the program *O* (Jones & Kjeldgaard, 1997). The final refinement rounds involved the placement of solvent molecules using the program *ARP* (Lamzin & Wilson, 1997). The resulting native DHDPS structure had $R_{\rm cryst}$ = 0.177 ($R_{\rm free}$ = 0.211), whereas the (*S*)-lysine-bound DHDPS structure had $R_{\rm cryst}$ = 0.159 ($R_{\rm free}$ = 0.186). In each case, there were two molecules in the asymmetric unit. Structure quality was assessed by means of *PROCHECK* (Laskowski *et al.*, 1993), which showed that in both structures 94.9% of the residues were in favourable regions, 4.7% in generously allowed regions and 0.4% in disallowed regions, where the offending residue was Tyr107, as previously described (Blickling *et al.*, 1997; Dobson, Valegård *et al.*, 2004; Mirwaldt *et al.*, 1995). The r.m.s.d. for the subunits in the asymmetric unit was 0.187 Å for the native structure and 0.181 Å for the (*S*)-lysine-bound structure, as calculated by means of *O* (Jones & Kjeldgaard, 1997). Data-collection and model-refinement statistics are summarized in Table 1.

3. Results and discussion

3.1. Structural features of native and (*S*)-lysine-bound DHDPS

3.1.1. General structural features. DHDPS from *E. coli* is a homotetramer (Shedlarski & Gilvarg, 1970) and the monomer is a $(\beta/\alpha)_8$-barrel (residues 1–224), where the active site is situated within the centre of the β-barrel (Figs. 3*a* and 3*b*). Each

monomer of DHDPS also has a C-terminal domain (residues 225–292) consisting of three α-helices, for which there is no known function. The quaternary structure reveals a dimer of dimers (monomers *A* and *B,* and monomers *C* and *D*; Fig. 3*c*) with strong connections between monomers *A* and *B* and rather weaker connections between the dimers. The asymmetric unit comprises the tight dimer. Neither structure shows any obvious change in its tertiary or quaternary architecture from that of the wild-type and mutant structures already determined (Blickling *et al.*, 1997; Dobson, Valegård *et al.*, 2004; Mirwaldt *et al.*, 1995). Elements of the tertiary structure are also highlighted in Fig. 3.

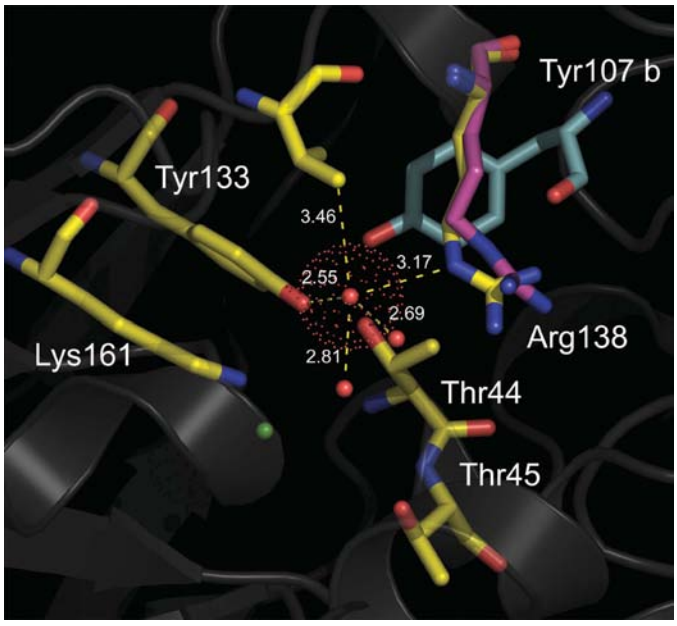

Figure 5
Reorientation of Arg138 and its connection to Tyr133 *via* a water molecule. Arg138 from the previously determined structure (PDB code 1dhp) is shown in purple. Distance calculations and the structure alignment with 1dhp were performed using *O* (Jones & Kjeldgaard, 1997).

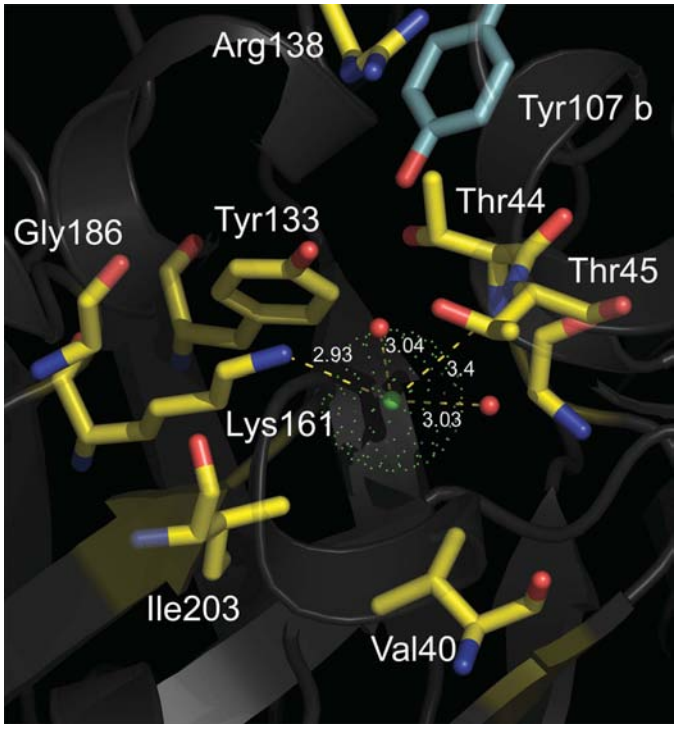

Figure 6
The position of the chloride ion near the active site of DHDPS.

3.1.2. Active site of DHDPS. Although similar to those previously published, the higher resolution structures presented here have real and important differences. In general, the architecture of the active site of the higher resolution structures is the same as that reported by Mirwaldt *et al.* (1995) and Blickling *et al.* (1997). Lys161, involved in Schiff-base formation, is placed within the β-barrel and Tyr133 sits above this residue (Fig. 4). Thr44 is hydrogen bonded to both Tyr133 and Tyr107; the latter tyrosine is provided by the other monomer of the tight-binding dimer, which reaches into the adjacent active site. This motif serves also as the terminus of a proton relay thought to shuttle protons to and from the active site to bulk solvent *via* a water-filled channel (Dobson, Valegård *et al.*, 2004). Each of these residues is highly conserved in all DHDPS enzymes known to date and catalytic activity is sensitive to mutation at any of these positions (Dobson, Valegård *et al.*, 2004). In addition, Tyr133 and Tyr107 are strictly conserved and Thr44 is conservatively substituted by serine within the *N*-acetyl neuraminate lyase subfamily of $(\beta/\alpha)_8$-barrel proteins, of which DHDPS is a member. The equivalent of Tyr133 is also proposed to play a central role in the catalytic cycle of neuraminate lyase (Lawrence *et al.*, 1997; Mirwaldt *et al.*, 1995). Unlike the solved structure of the DHDPS Tyr107Phe mutant (Dobson, Valegård *et al.*, 2004), where unexplained density was observed bound to Lys161 in the active site, all observed density in the active site of wild-type enzyme was consistent with water molecules and is modelled as such.

Situated at the entrance to the active site, Arg138 is thought to be essential for substrate binding: Blickling *et al.* (1997) have shown *via* structural studies that the guanidine of Arg138 will bind the carboxyl groups of (*S*)-ASA analogues. We find that Arg138 holds a different conformation (Fig. 5). Although still connected to the main-chain of Tyr107 of the other monomer in the dimer, the orientation of the guanidine of Arg138 is changed such that the N^{ε} atom makes a connection to the hydroxyl group of Tyr133 *via* a water molecule, rather than to the main-chain O atom of Tyr107. Thus, one N atom of the terminal guanidine is connected to the main-chain O atom of Tyr107, which presumably means that when binding the carboxyl group of (*S*)-ASA this connection must be broken. The projection of Tyr107 from one subunit into the active site of the other subunit requires that Tyr107 occupies a disallowed region of Ramachandran conformational space (Blickling *et al.*, 1997).

This is an important observation as it suggests that the guanidine moiety of Arg138 is more intimately involved in catalysis than first thought; the assessment of mutants of Arg138 will be helpful in answering this question. That the mutant DHDPS Tyr133Phe shows an increased K_m for

(*S*)-ASA (Dobson, Valegård *et al.*, 2004) offers circumstantial evidence for this assertion; without this Tyr133···Arg138 connection, Arg138 has become more flexible, as evidenced by the increased *B* factors observed for Arg138 in the DHDPS Tyr133Phe structure, thus affecting (*S*)-ASA binding. With wild-type and mutant structures all being crystallographically isomorphous, crystal-packing effects are much less likely to be responsible for changes in dynamics of this Arg138. When Arg138 is fixed by hydrogen bonding to Tyr133, there are only minor enthalpic and entropic consequences for this moiety on binding of (*S*)-ASA, whereas for the Tyr133Phe mutant the more mobile Arg138 now provides an unfavourable entropic contribution to the binding of (*S*)-ASA, lowering (*S*)-ASA affinity as observed. An intriguing corollary is whether the function of Tyr133 (and the proton relay) could be modulated by the binding of the carboxyl of (*S*)-ASA to the guanidine group of Arg138.

A large spherical peak of electron density close to active-site residue Lys161 is interpreted as a chloride ion (*B* value 24 Å^2, monomer *A*) on the basis of its contacts with the N$^{\varepsilon}$ atom of Lys161 (2.9 Å, *B* value 17 Å^2), the main-chain N atom of Thr44 (3.4 Å, *B* value 20 Å^2) and two water molecules that sit in the active site (both 3 Å, *B* values 20 and 25 Å^2; Fig. 6). A likely source for the chloride ion is the buffer solution (Tris–HCl), from which the protein solution was crystallized. This chloride ion was not observed by previous workers (Blickling *et al.*, 1997; Dobson, Valegård *et al.*, 2004; Mirwaldt *et al.*, 1995). However, a potassium ion, which has been noted in all published *E. coli* structures, is bound to the main-chain O atoms of residues 152, 154, 155 and 157, along with two well defined water molecules.

3.1.3. Re-evaluation of the dimer–dimer interface of *E. coli* DHDPS. The tight-dimer units of the *E. coli* DHDPS tetramer associate *via* two isologous interfaces formed between corresponding monomers of the dimer units. Published analyses of crystal structures of wild-type DHDPS report that intersubunit contacts at this dimer–dimer interface are comprised of only three amino-acid residues: Leu167, Thr168 and Leu197 (Blickling *et al.*, 1997; Mirwaldt *et al.*, 1995). This result was obtained using the program *CoPS* (unpublished program) with a distance cutoff of 3.9 Å. Additional to the three reported contacts, three new direct intersubunit contacts, involving five amino-acid residues and a water-bridging network, in which water molecules participate in intersubunit hydrogen bonding, were identified in our structure (Fig. 7). The dimer–dimer interface buries ∼1350 Å^2 (6.8% of surface area) for H_2O-stripped monomers, compared with ∼2250 Å^2 (11.3%) for the tight dimer.

Perhaps the most important of the newly identified contacts is a symmetrical pair of hydrogen bonds between the Gln196 residues of neighbouring subunits (Fig. 7*b*). In the published structure, the orientation of the N$^{\varepsilon}$ and O atoms of this residue is incorrect and the amide group should be rotated by 180°, producing the correct geometry for intermonomer hydrogen bonding between N$^{\varepsilon}$ and main-chain O atom of the neighbouring residue. This change also allows for formation of an intrasubunit hydrogen bond between the O$^{\varepsilon}$ atom of Gln196 and an NH_2 group of Arg230 from the same monomer.

Table 2
Connections and distances between (*S*)-lysine and the allosteric binding site.

(*S*)-Lysine	Residue	Distance (Å)
α-Carboxyl (O1)	Tyr106 OH	2.56
α-Carboxyl (O2)	Asn80 NH_2 (monomer *B*)†	3.29
α-NH_2	Ala49 main-chain O	2.78
α-NH_2	Asn80 carbonyl O (monomer *A*)	2.66
α-NH_2	Glu84 carbonyl O	2.65
ε-NH_2	His56 N	2.96
ε-NH_2	Ser48 main-chain O	2.67
ε-NH_2	H_2O	2.87

† Asn80 cross-links the monomers in the dimer *via* the (*S*)-lysine inhibitor.

Water-mediated hydrogen bonds are also formed between the two monomers at the interface. Asp193 has strong hydrogen bonds to two well defined water molecules that occupy cavities formed by the interface of the two monomers and are in turn hydrogen bonded to residues of the neighbouring monomer (Fig. 7*c*). One of these water molecules forms three separate hydrogen bonds to the other monomer, involving the main-chain N atom and the side-chain N$^{\varepsilon}$ atom of Asn171 and the main-chain O atom of Leu167. The second water molecule forms one further hydrogen bond to the main-chain O atom of Thr168 from the other monomer. Since Asp193 does not interact directly or indirectly with Asp193 from the neighbouring subunit, each interdimer interface contains two complete water-mediated hydrogen-bonding networks as described here.

The side chains of the two residues Glu175 and Gln234 protrude away from the surface of the monomer at the edge of the contact area between the two monomers and form hydrogen-bonded contacts that are separate from the main interface (Fig. 7*d*). These side chains are not constrained by other structural elements and are surrounded by solvent. They would therefore be expected to show flexibility and interact directly only transiently. This is borne out by the high *B* factors of these side chains indicated in the published structure. However, the correct geometry for hydrogen bonding between Glu176 O$^{\varepsilon}$ and the Gln234 N$^{\varepsilon}$ from the contacting subunit is conserved in all cases in the improved resolution structure, suggesting that this is an important intersubunit hydrogen bond.

Contact is also made at the interface by the side chains of Asn171 and Arg230 (Fig. 7*e*), which are positioned at the edge of the interface between the two monomers. The extremities of the side chains abut, resulting in close van der Waals contacts between the last four atoms of each side chain. Despite the presence of appropriate groups for hydrogen bonding, the geometric configuration of these groups does not lead to intersubunit hydrogen-bond formation and thus this contact is van der Waals in nature.

It is clear from this reinspection of the dimer–dimer interface that the number and range of contacts between the two monomers involved are much larger than the purely

hydrophobic interactions previously reported (Blickling *et al.*, 1997).

3.2. Overlay of native and (*S*)-lysine-bound structures

3.2.1. The allosteric binding site. (*S*)-Lysine is an allosteric modulator of DHDPS function, partially inhibiting catalytic activity. We have previously examined the kinetic details of *E. coli* DHDPS with respect to (*S*)-lysine inhibition (Dobson, Griffith *et al.*, 2004). Partial mixed inhibition was observed with respect to pyruvate (K_i = 3.9 ± 1.4 m*M*, K_i' = 0.18 ± 0.16 m*M*) and partial non-competitive inhibition with respect to (*S*)-ASA [K_i = 0.32 (± 0.03) m*M*]. However, the mechanisms responsible for inhibition are not well understood.

The (*S*)-lysine-binding site is situated in a crevice at the interface of the tight dimer, distal from the active site, but connected to the active site by a water channel (Fig. 8*a*). Initial inspection of the (*S*)-lysine-soaked structure showed positive electron density at the interface of the monomers in the tight dimer, indicating that (*S*)-lysine was indeed bound.

Of particular interest was an overlay of the structures of native and (*S*)-lysine-bound DHDPS. A surprising feature of such an overlay was the lack of changes between the two structures (r.m.s.d. for the overlay of the tight dimer was 0.17 Å); rather larger changes were reported for the wild-type and (S)-lysine-bound structures of the plant DHDPS from *N. sylvestris*. Not surprisingly, structural alterations are observed in the allosteric binding site upon (*S*)-lysine binding (Fig. 8*b*), as various residues move to accommodate the (*S*)-lysine molecule. Two (*S*)-lysine molecules bind in close proximity in the allosteric binding site. (*S*)-Lysine was found to have a similar orientation when compared with the lower resolution structure previously published and to make the same connections within the (*S*)-lysine-binding pocket, except that the N^{ε} atom was oriented differently and contacts the main-chain O atom of Ser48 instead of His53. Tyr106 moves towards the carboxyl group of (*S*)-lysine and thus the aromatic stack, comprising Tyr106 and Tyr107, has an altered conformation when compared with the native DHDPS structure. The connections and distances that (*S*)-lysine make to the tight dimer interface are shown in Table 2.

Previous structural studies have suggested that the function of Arg138 is to bind the carboxyl group of (*S*)-ASA (Blickling *et al.*, 1997). It was also proposed that one mode of inhibition by (*S*)-lysine may be to influence either (*S*)-ASA binding or cyclization, owing to rigidification of Arg138 (realised by a decrease in the *B* values for this side chain) upon (*S*)-lysine binding. Our (*S*)-lysine bound structure showed the opposite effect: the *B* values for Arg138 were noticeably increased when (*S*)-lysine was bound, indicating more flexibility than in the native structure. Indeed, whereas the averaged *B* value was the same in the lysine-bound and unbound structure, small increases (∼2–5 Å^2) in the *B* values were observed in the active-site residues for the lysine-bound structure. Moreover, as discussed above, Arg138 in each structure was bonded differently to the strained main chain of Tyr107. In previous *E. coli* DHDPS structures (Blickling *et al.*, 1997), the N^{ε} atom was bound to the main-chain O atom of Tyr107, but in the structures discussed here, the N^{ε} atom was bound *via* a water molecule to the hydroxyl group of Tyr133. Electron density was well resolved about this residue.

In order to detect changes in the conformation of the tetramer upon (*S*)-lysine binding, monomers *A* of DHDPS bound with and without (*S*)-lysine were overlaid (r.m.s.d. 0.15 Å). If the quaternary structure had changed, then monomer *D*, opposite monomer *A*, would be visibly displaced. Monomer *D* is only slightly displaced (less than 1 Å); thus, no significant quaternary change had occurred.

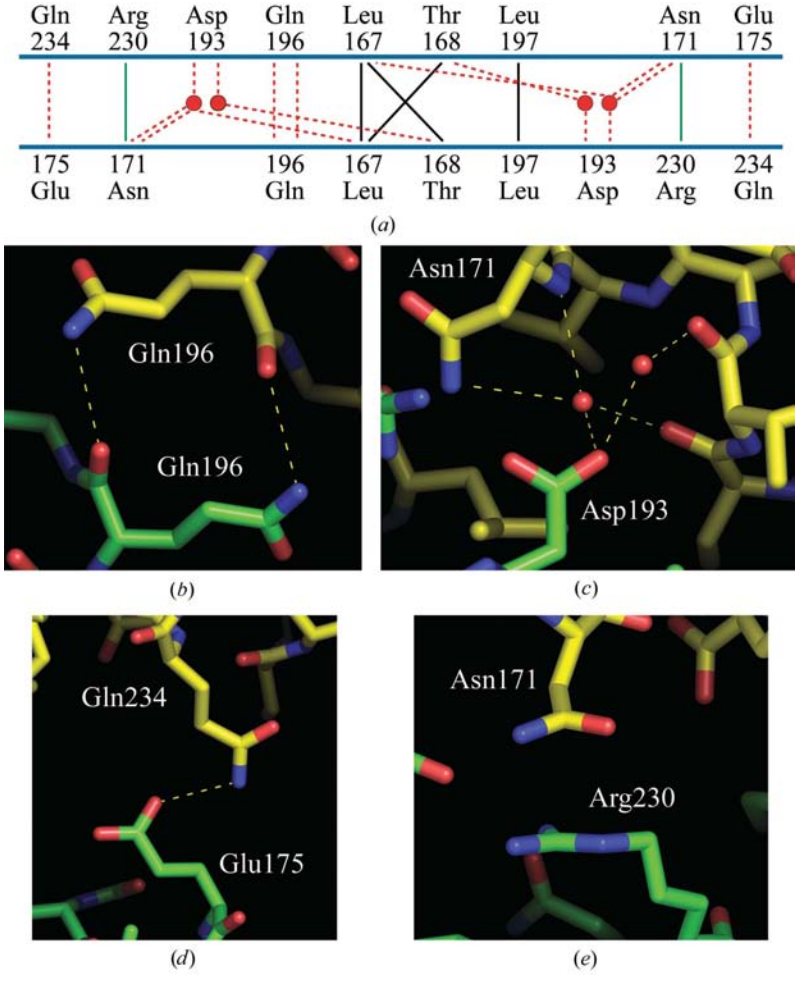

Figure 7
Re-evaluation of dimer–dimer interface. (*a*) Re-evaluation of the dimer–dimer interface of *E. coli* DHDPS. Hydrophobic contacts are indicated by black lines, van der Waals contacts are indicated by green lines and hydrogen bonds are indicated by dashed red lines. Water molecules are represented by red circles. (*b*) Hydrogen bonding between Gln196 residues from contacting subunits. (*c*) Water-mediated hydrogen bonds between two neighbouring subunits. (*d*) Hydrogen bonding between Gln234 and Glu175 of the neighbouring subunit. (*e*) Contact between Asn171 and Arg230 at the dimer–dimer interface.

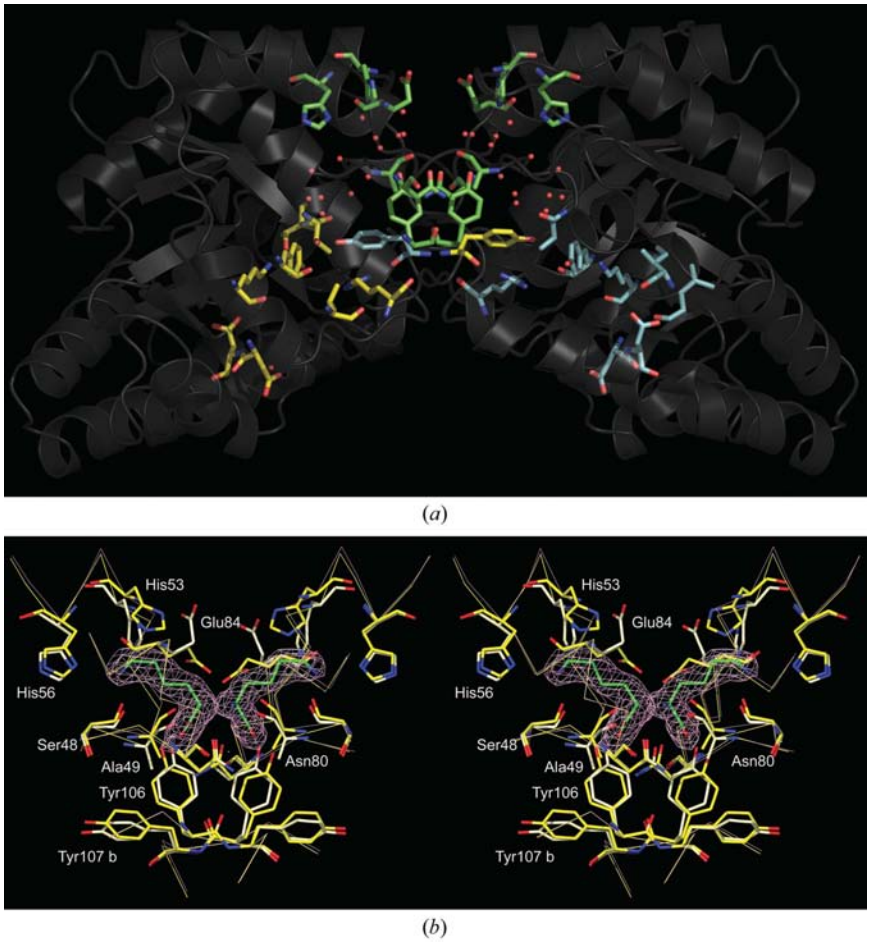

Figure 8
The (*S*)-lysine-binding site. (*a*) The (*S*)-lysine-binding site (residues in green) and its relationship to the active sites of the tight dimer (residues in blue and yellow). Waters in the channel connecting the active and (*S*)-lysine-binding sites are shown as red spheres. (*b*) Stereoview of an overlay of the allosteric binding site with and without bound (*S*)-lysine (green). Residues from the (*S*)-lysine-bound structure are shown in white, while those from the unbound structure are yellow. Electron density ($2F_o - F_c$, omit map) covers the two bound (*S*)-lysine ligands and is contoured at 1σ. This plot was produced using *O* (Jones & Kjeldgaard, 1997).

In addition to the (*S*)-lysine molecules found in the allosteric binding site, a third (*S*)-lysine was also identified. It was positioned at the entrance of the allosteric binding site, making contacts between two tetramers that are closely packed together and is thus likely to be a crystallographic artefact.

4. Conclusions

We have presented here a structural study of native *E. coli* DHDPS in order to elucidate and confirm the mechanisms of DHDPS as described by us and others. Higher resolution structures have enabled the observation of subtle features in the active-site residues, hinting at new mechanistic features which will be probed in future experiments. We find that globally our native structure differs little from those previously determined, but differences do appear on close examination. Of particular interest was the different conformation of Arg138 and its potential involvement in catalysis, other than the binding of (*S*)-ASA, *via* its connection with Tyr133. The dimer–dimer interface is more robust than previously described, but the role, if any, of the quaternary structure in the function of DHDPS remains unclear. In contrast, examination of the (*S*)-lysine-bound structure shows little change, apart from the presence of (*S*)-lysine at the allosteric binding site. However, contrary to previous reports, where the effect of (*S*)-lysine was to restrict Arg138, we find that Arg138 becomes more flexible upon (*S*)-lysine binding. Thus, the mechanism of (*S*)-lysine inhibition remains to be uncovered.

This work was funded by the Royal Society of New Zealand Marsden Fund (contract UOC303). Funding for the protein X-ray diffraction facility was provided in part by The Allan Wilson Centre for Molecular Ecology and Evolution. The authors wish to acknowledge Jackie Healy (University of Canterbury, New Zealand), Bryan Anderson and Jim Salvador (Massey University, New Zealand) for steadfast technical assistance and Peter Steel and Laurence Antonio (University of Canterbury, New Zealand) for passionate discussion/debate.

References

Bakhiet, N., Forney, F., Stahly, D. & Daniels, L. (1984). *Curr. Microbiol.* **10**, 195–198.
Bartlett, A. & White, P. (1986). *J. Gen. Microbiol.* **132**, 3169–3177.
Blickling, S., Beisel, H., Bozic, D., Knablein, J., Laber, B. & Huber, R. (1998). *J. Mol. Biol.* **274**, 608–621.
Blickling, S., Renner, C., Laber, B., Pohlenz, H.-D., Holak, T. A. & Huber, R. (1997). *Biochemistry*, **36**, 24–33.
Borthwick, E. B., Connel, S. J., Tudor, D. W., Robins, D. J., Shneier, A., Abell, C. & Coggins, J. R. (1995). *Biochem. J.* **305**, 521–524.
Collaborative Computational Project, Number 4 (1994). *Acta Cryst.* D**50**, 760–763.
Coulter, C. V., Gerrard, J. A., Kraunsoe, J. A. E., Moore, D. J. & Pratt, A. J. (1996). *Tetrahedron*, **52**, 7127–7136.
Coulter, C. V., Gerrard, J. A., Kraunsoe, J. A. E. & Pratt, A. J. (1999). *Pestic. Sci.* **55**, 887–895.
Cox, R. J., Sutherland, A. & Vederas, J. C. (2000). *Bioorg. Med. Chem.* **8**, 843–871.
Cremer, J., Eggeling, L. & Sahm, H. (1990). *Mol. Gen. Genet.* **229**, 478–480.
DeLano, W. L. (2002). *The PyMOL Molecular Graphics System.* DeLano Scientific, San Carlos, CA, USA. http://www.pymol.org.
Dereppe, C., Bold, G., Ghisalba, O., Ebert, E. & Schar, H.-P. (1992). *Plant Physiol.* **98**, 813–821.
Dobson, R. C. J., Gerrard, J. A. & Pearce, F. G. (2004). *Biochem. J.* **377**, 757–762.
Dobson, R. C. J., Griffin, M., Roberts, S. J. & Gerrard, J. A. (2004). *Biochimie*, **86**, 311–315.

Dobson, R. C. J., Valegård, K. & Gerrard, J. A. (2004). *J. Mol. Biol.* **338**, 329–339.
Frisch, D. A., Gengenbach, B. G., Tommey, A. M., Sellner, J. M., Somers, D. A. & Myers, D. E. (1991). *Plant Physiol.* **96**, 444–452.
Galili, G. (1995). *Plant Cell*, **7**, 899–906.
Galili, G. (2002). *Annu. Rev. Plant Biol.* **53**, 27–43.
Ghislain, M., Frankard, V. & Jacobs, M. (1990). *Planta*, **180**, 480–486.
Hoganson, D. & Stahly, D. (1975). *J. Bacteriol.* **124**, 1344–1350.
Hutton, C. A., Southwood, T. J. & Turner, J. J. (2003). *Mini Rev. Med. Chem.* **3**, 115–127.
Jones, T. & Kjeldgaard, M. (1997). *Methods Enzymol.* **277**, 173–208.
Karchi, H., Miron, D., Ben-Yaacov, S. & Galili, G. (1995). *Plant Cell*, **7**, 1963–1970.
Karsten, W. E. (1997). *Biochemistry*, **36**, 1730–1739.
Kumpaisal, R., Hashimoto, T. & Yamada, Y. (1989). *Agric. Biol. Chem.* **53**, 355–359.
Laber, B., Gomis-Rüth, F.-X., Româo, M. J. & Huber, R. (1992). *Biochem. J.* **288**, 691–695.
Lamzin, V. S. & Wilson, K. S. (1997). *Methods Enzymol.* **277**, 269–305.
Laskowski, R. A., MacArthur, M. W., Moss, D. S. & Thornton, J. M. (1993). *J. Appl. Cryst.* **26**, 283–291.
Lawrence, M. C., Barbosa, J. A. R. G., Smith, B. J., Hall, N. E., Pilling, P. A., Ooi, H. C. & Marcuccio, S. M. (1997). *J. Mol. Biol.* **266**, 381–399.
Mathews, B. & Widholm, J. (1978). *Planta*, **141**, 315–321.
Miflin, B. J., Napier, J. & Shewry, P. R. (1999). *Nature Biotechnol.* **17**, 13–14.
Mirwaldt, C., Korndorfer, I. & Huber, R. (1995). *J. Mol. Biol.* **246**, 227–239.
Navaza, J. & Saludjian, P. (1997). *Methods Enzymol.* **276**, 581–594.
Pflugrath, J. W. (1999). *Acta Cryst.* D**55**, 1718–25.
Shedlarski, J. G. & Gilvarg, C. (1970). *J. Biol. Chem.* **245**, 1362–1373.
Stahly, D. P. (1969). *Biochim. Biophys. Acta*, **191**, 439–451.
Tosaka, O. & Takinami, K. (1978). *Agric. Biol. Chem.* **42**, 95–100.
Tudor, D. W., Lewis, T. & Robins, D. J. (1993). *Synthesis*, pp. 1061–1062.
Wallsgrove, R. M. & Mazelis, M. (1981). *Biochemistry*, **20**, 2651–2655.
Webster, F. & Lechowich, R. (1970). *J. Bacteriol.* **101**, 118–126.
Yamakura, F., Ikeda, Y., Kimura, K. & Sasakawa, T. (1974). *J. Biochem.* **76**, 611–621.
Yugari, Y. & Gilvarg, C. (1965). *J. Biol. Chem.* **240**, 4710–4716.